| Title | Electrocatalytic activity and volatile product selectivity for nitrate reduction at tin-modified Pt(100), Pd(100) and Pd–Pt(100) single crystal electrodes in acidic media |
|---|---|
| Author(s) | Kato, Masaru; Unuma, Yuki; Okui, Manabu; Qu, Yunteng; Zheng, Jinhang; Taguchi, Satoshi; Kiguchi, Fumiya; Torihata, Mashu; Gao, Yunzhi; Hoshi, Nagahiro; Yagi, Ichizo |
| Citation | Electrochimica Acta, 398, 139281<br>https://doi.org/10.1016/j.electacta.2021.139281 |
| Issue Date | 2021-12-01 |
| Doc URL | http://hdl.handle.net/2115/90759 |
| Rights | © 2021. This manuscript version is made available under the CC-BY-NC-ND 4.0 license http://creativecommons.org/licenses/by-nc-nd/4.0/ |
| Rights(URL) | http://creativecommons.org/licenses/by-nc-nd/4.0/ |
| Type | article (author version) |
| Additional Information | There are other files related to this item in HUSCAP. Check the above URL. |
| File Information | PtPd_DEMS_manuscript.pdf |

**Electrocatalytic activity and volatile product selectivity for nitrate reduction at tin-modified Pt(100), Pd(100) and Pd–Pt(100) single crystal electrodes in acidic media**

Masaru Kato,[a,b*] Yuki Unuma,[b] Manabu Okui,[b] Yunteng Qu,[c†] Jinhang Zheng,[b] Satoshi Taguchi,[e] Fumiya Kiguchi,[d] Mashu Torihata,[d] Yunzhi Gao,[c] Nagahiro Hoshi,[d] Ichizo Yagi [a,b*]

[a]Faculty of Environmental Earth Science and [b]Graduate School of Environmental Science, Hokkaido University, N10W5, Kita-ku, Sapporo 060-0810, Japan

[c]School of Chemistry and Chemical Engineering, Harbin Institute of Technology, No. 92 West-Da Zhi Street, Harbin 150001, People's Republic of China

[d]Department of Applied Chemistry and Biotechnology, Graduate School of Engineering, Chiba University, Yayoi-cho 1-33, Inage-ku, Chiba 256-8522, Japan

[e]Laboratory of Chemistry, Hokkaido University of Education Sapporo, Ainosato 5-3-1, Kita-ku, Sapporo 002-8502, Japan

†Present address: State Key Laboratory of Photoelectric Technology and Functional Materials, International Collaborative Center On Photoelectric Technology and Nano Functional Materials, Institute of Photonics and Photon-Technology, Northwest University, Xi'an 710069, People's Republic of China

**Corresponding authors**

*E-mail: masaru.kato@ees.hokudai.ac.jp (MK); iyagi@ees.hokudai.ac.jp (IY)

**Abstract**

We prepared Sn-modified Pt(100), Pd(100) and Pd–Pt(100) single crystal electrodes and investigated the nitrate reduction reaction ($NO_3RR$) activity and the product selectivity for them using online electrochemical mass spectroscopy (OLEMS), also known as differential electrochemical mass spectroscopy (DEMS). OLEMS measurements allowed us to quantify volatile products of $N_2$, $N_2O$ and NO and confirm the production of $N_2$ at Sn/Pd(100) but not at Sn/Pt(100). Pd-doping to Pt(100) with a 3 atomic % increased the product selectivity for the $NO_3RR$ to $N_2$. These results indicate that the presence of Pd in the (100) surface is the key to produce $N_2$, which seems to be related to the hydrogen adsorption energy to the metal surface. The suppression of hydrogenation of intermediate species at the electrode surface could lead to the production of $N_2$. This work will guide us to understand $N_2$ production mechanism for the $NO_3RR$ and develop highly selective electrocatalysts for denitrification.

# 1. Introduction

Nitrate ($NO_3^-$) ions can be converted in natural biological processes including microbial denitrification to various inorganic compounds such as nitrite ($NO_2^-$) ions, nitric oxide (NO), nitrous oxide ($N_2O$), hydroxylammonium ions ($NH_3OH^+$), ammonium ions ($NH_4^+$) and dinitrogen ($N_2$). While many of these processes are essential to life, agricultural runoff and industrial waste streams can cause accumulation of excess $NO_3^-$ and $NO_2^-$ in groundwater, leading to negative impacts on global environments such as algal blooms, global warming and ozone layer depletion [1-3] and human health including methemoglobinemia (blue baby syndrome) and cancer [4,5]. To purify nitrate-contaminated groundwater or industrial water, electrocatalytic denitrification is a promising technology [5-8].

Electrocatalytic denitrification processes have advantages over thermocatalytic or biological processes because they require no additional chemical, can operate at ambient temperature and pressure, and can be powered by renewable energy [5-8]. Noble metal electrodes modified with p-block elements are known to show high electrocatalytic activity for the nitrate reduction reaction ($NO_3RR$). Sn is the most active promotor in the p-block elements for noble metal electrodes such as Pt [9-12] and Pd [10,12-14]. The surface modification of these noble metals with Sn accelerates the initial rate-determining step for the $NO_3RR$, $NO_3^-$ to $NO_2^-$. Although Sn-modified Pt or Pd

4

electrodes have been widely studied for the electrocatalytic NO$_3$RR improvement, the exclusive production of the most environmentally friendly product dinitrogen (N$_2$) remains challenging.

Single crystal electrodes with low index surfaces provide us with a powerful platform to understand fundamental insights into the relationship of the surface structure with electrocatalytic activity and product selectivity. For the NO$_3$RR, Sn-modified Pt(100) electrodes tend to show higher electrocatalytic activity than Sn-modified Pt(111) electrodes [10]. For the NO$_2^-$ reduction, the catalytic activity of single crystal platinum electrodes increases in the following order: Pt(111)<Pt(110)<<Pt(100) [5]. Density functional theory (DFT) calculations suggest that N–N bond formation can occur with lower barriers on the square lattice of the (100) surface as compared to the hexagonal (111) surface [15-17]. Furthermore, quasi-perfect Pt(100) surfaces are also unique in their sensitivity, achieving the direct conversion of NO$_2^-$ to N$_2$ in alkaline solution [18,19]. These results encourage us to investigate the electrocatalytic activity and product selectivity of Sn-modified Pt(100) electrodes for the NO$_3$RR in acidic media. Compared with Pt electrodes, Pd electrodes are known to reduce NO to N$_2$ not only in alkaline media but also in acidic media [20]. Sn/Pd electrodes have a stronger tendency to the N–N bond formation than Sn/Rh, Sn/Pt and Sn/Ir [12], and Pd is one of the best (and few) catalysts for the N$_2$O reduction to N$_2$ with ~100% Faradaic

efficiency [21-23]. However, there is no report on the activity and selectivity of Sn-modified Pd(100) electrodes for the electrochemical NO$_3$RR.

Herein, we report the preparation of Sn-modified Pt(100), Pd(100) and Pd–Pt(100) electrodes and the analysis of gas species produced at them during the electrocatalytic NO$_3$RR in acidic media. To quantify the volatile products of NO, N$_2$O and N$_2$, an online electrochemical mass spectrometry (OLEMS), also known as differential electrochemical mass spectroscopy (DEMS), was used. The OLEMS is a powerful technique to detect volatile products produced at electrodes during electrochemical measurements [9,13,24]. The quantification of the volatile products allowed us to discuss the difference in the NO$_3$RR product selectivity between Pt(100) and Pd(100) and the effect of Pd-doping to Pt(100) on the product selectivity to N$_2$.

## 2. Experimental section

### 2.1. Materials

Perchloric acid (70%, purity: 99.999%; Sigma-Aldrich), sulfuric acid (99.999%, Sigma-Aldrich), tin(II) chloride dihydrate (97.0%, Kanto Chemical) and sodium nitrate (99.99%, Kanto Chemical) were purchased and used without further purification. Platinum wires (0.8 mm$\phi$ or 0.5 mm$\phi$; 99.99% purity) and palladium (0.8 mm$\phi$ or 0.5 mm$\phi$; 99.99% purity) wires were used for the preparation of single crystal electrodes.

Thin GORE PTFE membranes (VE91221, 0.32 mm in thickness) were provided by W.

L. Gore & Associates. POREFLON membranes (HP-010-30; pore size: 0.1 µm;

thickness: 30 µm) were provided by Sumitomo Electric Fine Polymer.

## 2.2. Preparation of single crystal electrodes

Pt, Pd and Pd–Pt alloy single crystal beads were prepared based on the procedure

previously reported [10]. A platinum wire or a palladium wire was annealed in methane-

oxygen flame to obtain a single crystal bead at the end of the wire. For the preparation

of Pd–Pt alloy single crystal beads with 3 atomic % (at %) of Pd in Pt, a single crystal

bead of Pt was used as a seed crystal as well as the source of Pt, and an amount of Pd

was added to the Pt bead in methane-oxygen flame. The single crystal beads were

oriented using the reflection of a He–Ne laser beam from a (100) facet on the single

crystal bead, fixed in a poly(methyl methacrylate) resin (Technovit 4004, Heraeus

Kulzer), cut in the direction of the (100) facet, and then polished with diamond slurries

to be mirror-finished. The polished single crystal electrode was annealed in methane-

oxygen flame at <1250 °C for 4 h. To confirm the preparation of the single crystal

electrode with a specific orientation, cyclic voltammograms (CVs) were recorded in 0.5

M $H_2SO_4$ aqueous solution under Ar.

## 2.3. Electrochemical measurements

A glass-tubing chamber that has a gas inlet at the bottom and a gas outlet at the top was used for annealing electrodes. This chamber can keep Milli-Q water at the bottom. The Pt single crystal electrodes were annealed under $H_2$–Ar in the glass-tubing chamber that is placed in an induction coil of an induction heating system (EASY-HEAT model 0224, Ambrell), cooled under $H_2$–Ar, and then immersed in Milli-Q water purged with Ar in the same chamber. The surface of the electrode was covered with Milli-Q water and then transferred to the electrochemical cell for electrochemical measurements. Similarly, Pd and Pd–Pt alloy single crystal electrodes were annealed using the induction heating system. Pd–Pt electrodes were cooled and then immersed in Milli-Q water under $H_2$-Ar whereas Pd electrodes under Ar. The annealed electrode covered with a droplet of Milli-Q water was transferred to the electrochemical cell for electrochemical measurements. All electrochemical data were recorded on potentiostats (HZ7000, Hokuto Denko) equipped with a high-current booster (HZAP3003A, Hokuto Denko) using conventional three-electrode systems under Ar (99.999%, HOKKAIDO AIR WATER) with a Ag|AgCl (sat. KCl) electrode with a double junction holder (International chemistry) as the reference electrode and platinum foil coated with platinum black as the counter electrode. Single crystal electrodes were used as the working electrode. Electrolyte solutions were purged with Ar (99.999%) for at least 30 min before measurements. All electrochemical measurements were performed in the

hanging meniscus configuration. CVs on nitrate reduction were recorded in a 0.1 M

HClO$_4$ aqueous solution containing 0.1 M NaNO$_3$ at a sweep rate of 10 mV s$^{-1}$ under

Ar. All potentials in the main text are shown against the reversible hydrogen electrode

(RHE). The potentials against Ag|AgCl (sat. KCl) were converted to those against RHE

using the following equation: $E$ (*vs.* RHE) = $E$ (*vs.* Ag|AgCl (sat. KCl)) +0.199 V +

0.059 V × pH.

The surface modification of single crystal electrodes with tin was carried out based

on a reported procedure [10]. The annealed single crystal electrode covered with a

droplet of Milli-Q water was immersed in 0.1 M HClO$_4$ aqueous solution containing 0.5

mM SnCl$_2$ for 30 s and then the electrode was immersed in Milli-Q water under Ar to

remove excess tin species from the surface. The tin-modified electrode covered with a

droplet of Milli-Q water was transferred to the electrochemical cell. CVs of tin-

modified electrodes in the Hupd desorption region in 0.5 M H$_2$SO$_4$ aqueous solution

allowed us to determine the tin surface coverage ($\theta_{Sn}$) using the following equation: $\theta_{Sn}$

= $(Q_H{}^0 - Q_H)/Q_H{}^0$ , where $Q_H{}^0$ and $Q_H$ indicate the Faradaic charges corresponding to

the desorption of H$_{upd}$ before and after the tin modification, respectively.

**Auger electron spectroscopy**

Auger electron spectra were recorded in a derivative mode on JAMP-9500F (JEOL)

using the 10 keV electron beam energy, 1 eV modulation, and 10 nA beam current in

the range from 30 to 2500 eV.

**Online electrochemical mass spectrometry (OLEMS) system.**

An OLEMS setup was constructed according to the literature [25]. The OLEMS

setup consists of a quadrupole mass spectrometer (M201QA-TDM, CANON

ANELVA), metal ionization gauge (GI-M2, ULVAC), a rotary vane vacuum pump

(GLD-135, ULVAC) and a turbo molecular vacuum pump (5150 Turbo Pump, Alcatel)

equipped with a controller (CFF450, Alcatel). A glass pinhole was used as the gas inlet

to the mass spectrometer. This pinhole was covered with a thin GORE PTFE membrane

(VE91221, 0.32 mm in thickness) and a POREFLON membrane (HP-010-30; pore size:

0.1 µm; thickness: 30 µm) and then heated with a heat gun. The inner diameter of the

pinhole was below 10 µm. The working electrode was set in the hanging meniscus

configuration and the pinhole was placed underneath the electrode surface within 30

µm. The internal pressure was $3$–$4 \times 10^{-4}$ Pa during the OLEMS experiments.

**Product analysis for electrocatalytic nitrate reduction.**

The single crystal electrode used was annealed in the same procedure for standard

electrochemical measurements. To confirm the clean surface of the electrode, CVs were

recorded in 0.5 M degassed $H_2SO_4$ aq. Sweep rates were 50 mV s$^{-1}$ for Pt and Pd–Pt

alloy electrodes and 20 mV s$^{-1}$ for Pd electrodes. After the electrochemical measurements in 0.5 M H$_2$SO$_4$ aq. under Ar, the electrode covered with a droplet of 0.5 M H$_2$SO$_4$ aq. was transferred to a degassed 0.1 M HClO$_4$ aqueous solution containing 0.5 mM SnCl$_2$ and then kept in the solution for 30 s. The electrode covered with a droplet of the SnCl$_2$ solution was to a degassed Milli-Q water and then cleaned in it. The electrode covered with Milli-Q water was transferred again to 0.5 M degassed H$_2$SO$_4$ aq. to record CVs again and confirm the surface modification with Sn species. Note that all solutions used in the above processes were degassed with Ar for at least 30 min.

For OLEMS, an electrolyte aqueous solution containing 0.1 M HClO$_4$ and 0.1 M NaNO$_3$ was used. This solution was purged with Ar for at least 30 min before use. The tin-modified electrode covered with a drop of 0.5 M degassed H$_2$SO$_4$ aq. was transferred to a degassed Milli-Q water and then cleaned in it. The electrode covered with a drop of Milli-Q water was transferred to the 0.1 M HClO$_4$ solution containing NaNO$_3$ under Ar. CVs were recorded at a sweep rate of 1 mV s$^{-1}$ from +0.40 to –0.05 V and then +0.40 V vs. RHE under Ar.

Although quantitative analysis of OLEMS data remains challenging, we roughly quantified amounts of gasous products for the NO$_3$RR, and then calculated Faradaic

efficiencies of the production of them. The details are described in the Supplimentary

Data.

## 3. Results and discussion

### 3.1 Characterization of Pt(100), Pd(100) and Pd–Pt(100).

To confirm the preparation of Pt(100) electrodes, CVs of Pt(100) were recorded in a

0.5 M $H_2SO_4$ aqueous solution under Ar (**Fig. 1a**). The symmetric CV indicates that the

electrochemical processes on the surface were reversible [26]. Characteristic waves in

the potential range between +0.2 and +0.45 V vs. RHE are associated with adsorption

and desorption of underpotentially deposited hydrogen, $H_{upd}$ [27]. The sharp peak at

+0.37 V vs. RHE is associated with extended (1x1)–Pt(100) long-range order [28]. The

peak at +0.27 V vs. RHE was assigned to defect sites at the edge of (100) terraces [29].

These electrochemical features allowed us to confirm the successful preparation of

Pt(100) electrodes.
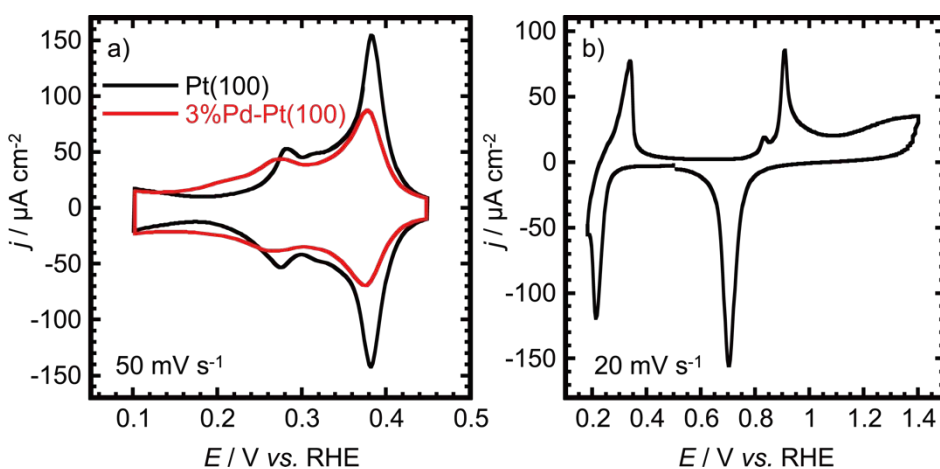
**Fig. 1** Representative CVs of (a) Pt(100) (the trace in black) and 3 at % Pd–Pt(100) (the trace in red) and (b) Pd(100). CVs were recorded at a sweep rate of 50 mV s$^{-1}$ for Pt(100) and Pd–Pt(100) and 20 mV s$^{-1}$ for Pd(100) in a 0.5 M H$_2$SO$_4$ aqueous solution under Ar.

CVs of Pd(100) were also recorded in a 0.5 M H$_2$SO$_4$ aqueous solution under Ar (**Fig. 1b**). A sharp anodic peak at ca. +0.35 V vs. RHE and a sharp cathodic peak at ca. +0.22 V were observed and associated with desorption and adsorption of sulfate anions, respectively [30,31]. At ≤ ca. +0.3 V vs. RHE, cathodic currents involving hydrogen absorption into palladium bulk are known to overlap with the adsorption of sulfate anions. We also observed anodic and cathodic peaks at ca. +0.90 and +0.73 V vs. RHE, respectively. These are assigned to be the formation of the surface oxide and reduction of it, respectively. The peak potential of the Pd surface oxide formation is sensitive to the surface structure: the higher the surface atomic density is, the more positive the peak position of the oxide formation is [30,32]. The peak potential observed was in good agreement with Pd(100) single crystal electrodes previously reported [30], allowing us to confirm the preparation of Pd(100) electrodes.

We prepared Pd-Pt(100) electrodes with a 3 at % of Pd in Pt. Pd was added into a Pt bead as the seed crystal in methane–oxygen flame to prepare a Pd–Pt alloy single crystal bead because the melting point of Pt (2041 K) is higher than that of Pd (1828 K) and the melting seed crystal must retain to obtain a uniform alloy *via* the convection of the molten metal [33]. A representative CV of the prepared Pd–Pt(100) electrode was

shown in **Fig. 1a**. Although the Pd–Pt(100) showed a similar redox behavior to Pt(100), the peak intensity at ca. +0.37 V decreases, and the peak position shifts to more negative potentials, compared with the CV of Pt(100). Furthermore, such negative peak shifts were also observed for hydrogen adsorption/desorption peaks at (100) terrace edges at ca. +0.27 V. These results indicate that the Pd–Pt alloy formation weakens the Pt–H bonding for the $H_{upd}$ at the surface. Similar changes were already reported for Pd–Pt(100) alloy electrodes with different bulk compositions [28,34]. An Auger electron spectrum of Pd–Pt(100) (**Fig. S1**) indicated that the pure Pt(100) was replaced by surface alloy phases for Pd–Pt(100) alloys. This spectrum also enabled us to determine an atomic percentage of Pd at the surface to be ca. 12 at %, which was greater than 3at % in the bulk. For previously prepared Pd–Pt(100) single crystal electrodes, the amount of palladium at the surface for Pd–Pt(100) was also greater than that in the bulk [28]. Thus, it is most likely that the amount of palladium at the surface of Pd–Pt(100) that we prepared is also greater than that in the bulk.

**3.2 Electrocatalytic NO₃RR at Sn/Pt(100), Sn/Pd(100) and Sn/Pd–Pt(100) electrodes.**

CVs of tin-modified and unmodified Pd(100) electrodes were recorded in the presence of nitrate under Ar to understand the electrocatalytic NO₃RR activity (**Fig.**

**2b**). This is the first report on the electrocatalytic $NO_3RR$ for Sn/Pd(100) electrodes and therefore we collected CVs particularly for tin-modified Pd(100) electrodes with different surface coverages of tin ($\theta_{Sn}$). The surface of Pd(100) electrodes was modified with tin species, which are possibly composed of metallic Sn and $Sn^{II}(OH)_x$ species [10,11], and then tin surface coverages ($\theta_{Sn}$) were determined based on the hydrogen desorption peak (**Fig. S2**) [10]. With low $\theta_{Sn}$ values, Pd(100) showed almost no catalytic currents whereas cathodic currents involving $NO_3RR$ were observed for the Pd(100) electrodes with $\theta_{Sn} = 0.71$ and 0.91 (**Fig. S3**). This activity dependence on $\theta_{Sn}$ is similar to those previously reported tin-modified palladium electrodes [14]. The Sn/Pd(100) electrodes with $\theta_{Sn} = 0.71$ and 0.91 showed almost the same catalytic current densities of ca. $-16$ mA cm$^{-2}$ at 0.01 V vs. RHE. In the negative-going sweep, cathodic currents increased and maximized at ca. 0.13 V vs. RHE but decreased at $<$ 0.13 V vs. RHE for Sn/Pd(100) electrodes with $\theta_{Sn} = 0.71$ and 0.91. Similar deactivation processes were also observed at potentials lower than 0.12 V for tin-modified platinum electrodes including Sn/Pt(poly) [9,35], Sn/Pt(111) and Sn/Pd–Pt(111) with low $\theta_{Sn} \leq 0.4$ [10]. The deactivation of these electrodes is associated with the formation of strongly adsorbed hydrogen on platinum [9]. Interestingly, the deactivation for Sn/Pd(100) was observed even with high $\theta_{Sn}$ of 0.71 and 0.91 (**Figs. 2b and S3**), indicating that specific adsorption processes of other species could be

involved: for example, nitric oxide is known to adsorb on metal surfaces including

platinum [36,37]. Because no such deactivation was observed for Sn/Pt(100) and Sn/Pd–

Pt(100) electrodes, the nitrate reduction activity on Sn/Pd(100) is highly sensitive to the
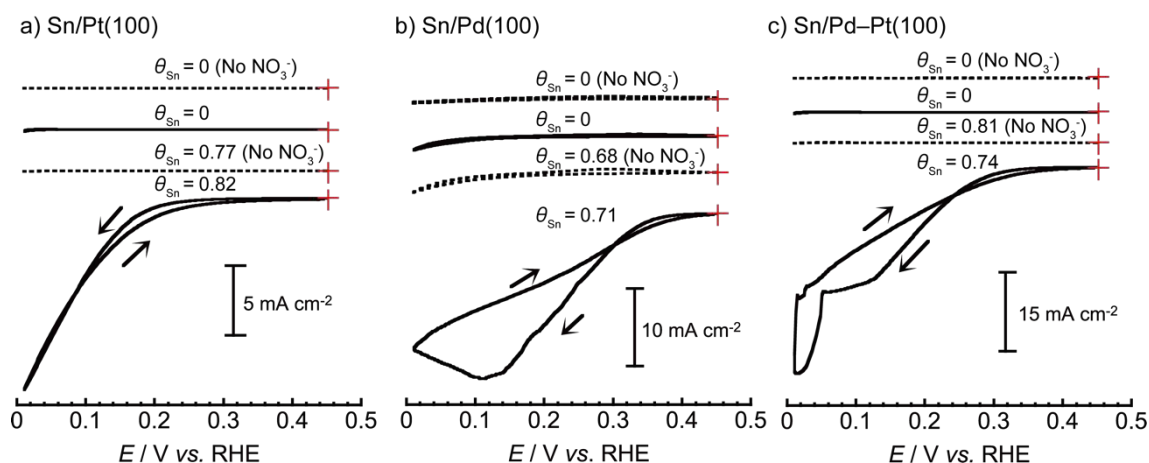
specific adsorption of products.



**Fig. 2** CVs of (a) Sn/Pt(100), (b) Sn/Pd(100) and (c) Sn/Pd–Pt(100) recorded at 10 mV
s$^{-1}$ in a 0.1 M HClO$_4$ aqueous solution in the presence (the solid lines) and the absence
(the broken lines) of 0.1 M NaNO$_3$ under Ar. Arrows in black and plus signs in red
indicate the sweep direction and the initial position of the CV, respectively.

We also prepared Sn/Pt(100) and Sn/Pd–Pt(100) electrodes based on the preparation

procedure previously reported [10]. Although unmodified Pt(100) and Pd–Pt(100)

electrodes are known to show the NO$_3$RR activity [38], their activities were much lower

than those of tin-modified electrodes (**Figs. 2a and 2c**). Thus, the tin-modification gave

a drastic increase of the NO$_3$RR activity to Pt(100) and Pd–Pt(100) electrodes. Since a

tin coverage range between 0.7 to 0.8 maximized the electrocatalytic NO$_3$RR activity

for tin-modified (100) electrodes we prepared in this work, we used Sn/Pt(100) and

Sn/Pd-Pt(100) electrodes with $\theta_{Sn} \sim 0.75$ for the further studies.

### 3.3 Product analysis of electrocatalytic NO₃RR using OLEMS.

To analyze products for the electrochemical $NO_3RR$ produced at single crystal

electrodes, an online electrochemical mass spectroscopy (OLEMS) setup, also known as

differential electrochemical mass spectroscopy (DEMS), was constructed as shown in

**Fig. 3** [25]. In our setup, the glass pinhole, which was covered with porous PTFE

membranes, was placed close to the surface of the working electrode and used as the gas

inlet to the mass spectrometer to analyze gaseous products (**Fig. 3b**).
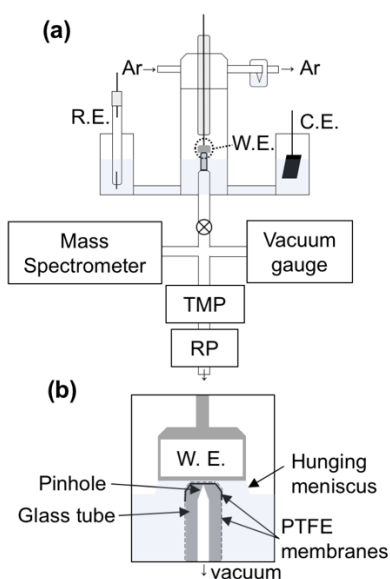


**Fig. 3**. The OLEMS setup used in this work.

LSVs and OLEMS results allowed us to understand the potential dependence of

volatile products of NO, $N_2O$ and $N_2$ for Sn/Pt(100), Sn/Pd(100) and Sn/Pd–Pt(100)

electrodes (**Fig. 4**). All electrodes showed cathodic currents for the NO$_3$RR at <0.3 V

vs. RHE (**Fig. 4a**) and associated mass signals for the volatile products also increased at

<0.3 V vs. RHE (**Fig. 4b–c**). Although quantitative analysis of OLEMS data remains

challenging, we approximately quantified amounts of volatile products and then

calculated Faradaic efficiencies of them (See more details in the Supplementary data).

Our calculation indicates that the Sn/Pt(100) electrode produced volatile products of NO

and N$_2$O with a Faradaic efficiency of ca. 25% (**Fig. S6a**), indicating that non-volatile

products of NH$_3$ and NH$_2$OH, which was reported as the main product for tin-modified

platinum polycrystalline electrodes [39], were mainly produced at Sn/Pt(100) rather

than the volatile products. It is most likely that H$_{upd}$ atoms on the Pt surface are

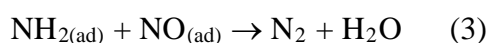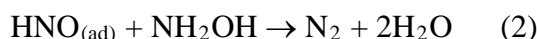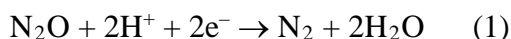involved in the production of non-volatile products [11,40,41].
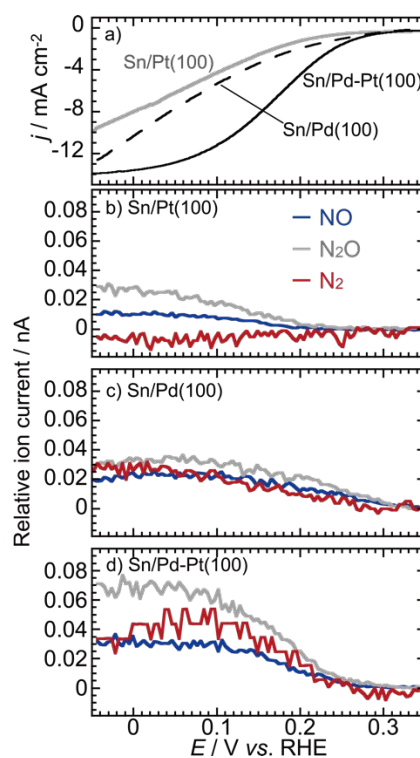
**Fig. 4** (a) Linear sweep voltammograms recorded in the negative-going sweep at 1 mV $s^{-1}$ in a 0.1 M $HClO_4$ aqueous solution containing 0.1 M $NaNO_3$ under Ar and the associated mass signals of NO (the traces in blue), $N_2O$ (the traces in gray) and $N_2$ (the traces in red) for (b) Sn/Pt(100), (c) Sn/Pd(100) and (d) Sn/Pd–Pt(100). The tin coverages of $\theta_{Sn}$ for Sn/Pt(100), Sn/Pd(100) and Sn/Pd–Pt(100) were 0.80, 0.71 and 0.82, respectively.

In contrast to Sn/Pt(100), Sn/Pd(100) produced not only NO and $N_2O$ but also $N_2$ (**Fig. 4c**). A Faradaic efficiency for the production of these gases reached ca. 92% at +0.2 V vs. RHE and $N_2$ accounted for 34% (**Fig. S6b**). At polycrystalline palladium electrodes, $N_2$ was produced for the electrochemical nitric oxide reduction in acidic media but not at polycrystalline platinum electrodes [20]. Thus, the efficient reduction of NO to $N_2$ proceeds at the Pd(100) surface rather than the production of non-volatile products. Interestingly, Faradaic efficiencies of the total gaseous products dropped from 92% at 0.2 V vs. RHE to ca. 50% at $\leq$ 0.15 V vs. RHE for Sn/Pd(100) (**Fig. S6b**) but still higher than those obtained for Sn/Pt(100) (**Fig. S6a**). The formation of non-volatile products such as $NH_2OH$ [13] could be suppressed at Sn/Pd(100), compared with Sn/Pt(100), even in the $H_{upd}$ potential range (**Fig. 1b**).

The 3% doping of Pd into Pt(100) gave a huge impact on the product distribution and produced $N_2$ (**Fig. 4d**), which was not detected for Sn/Pt(100) (**Fig. 4b**). Sn/Pd–Pt(100) produced the volatile products with a Faradaic efficiency of ca. 60% in the potential range between 0.1 and 0.2 V vs. RHE (**Fig. S6c**). Compared with Sn/Pt(100),

the Sn/Pd–Pt(100) electrode suppressed the formation of non-volatile products such as

$NH_2OH$ or consecutively converted them to $N_2$.

For the formation of $N_2$ for the $NO_3RR$ at Pt and Pd electrodes, four reaction

pathways have been proposed [4-7,9]:

$$N_2O + 2H^+ + 2e^- \rightarrow N_2 + 2H_2O \quad (1)$$

$$HNO_{(ad)} + NH_2OH \rightarrow N_2 + 2H_2O \quad (2)$$

$$NH_{2(ad)} + NO_{(ad)} \rightarrow N_2 + H_2O \quad (3)$$

$$2N_{(ad)} \rightarrow N_2 \quad (4)$$
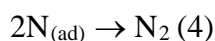
$N_2O$ can be reduced to $N_2$ at Sn/Pd–Pt(100) following Reaction (1). $N_2O$ can be formed

*via* an electrocatalytic dimerization between $NO_{(ad)}$ at the surface and $NO_{(aq)}$ in solution

in an Eley-Rideal-like mechanism [20] rather than the Langmuir-Hinshelwood-like

mechanism between two $NO_{(ad)}$ species [42]. Reaction (1) can be responsible for $N_2$

production during the nitrate reduction even at Sn-modified Pt electrodes particularly in

long-term electrolysis experiments, where it proceeds at the remaining free Pt sites

[9,35]. Since Pd efficiently drives the electrocatalytic $N_2O$ reduction to $N_2$ [21,22],

Reaction (1) can be accelerated at Sn/Pd–Pt(100), compared with Sn/Pt(100). $N_2O$ has

moderate solubility in water ($\sim$24 mmol $L^{-1}$) [3,43] and solubilized $N_2O$ can be

susceptible to be reduced after re-adsorption [7,44].

Another plausible reaction pathway at Sn/Pd–Pt(100) is Reaction (2): NO adsorbed

on the electrode surface ($NO_{(ad)}$) can be converted to $NH_2OH$ *via* $HNO_{(ad)}$, where

$NH_2OH$ could react with $HNO_{(ad)}$ to produce $N_2$ and $H_2O$ [6,7,43]. This reaction

pathway was proposed as one of the plausible pathways for a tin cathode [43]. Although

there is no experimental confirmation of the production of $NH_2OH$ in this work,

$NH_2OH$ can be produced at Sn/Pt(100) because tin-modified polycrystalline platinum

electrodes are known to produce $NH_2OH$ as the main product in the non-volatile

products [39]. Reaction (2) occurs even in acidic media, where $NH_2OH$ should be

hydroxylammonium ($NH_3OH^+$) [9].

Reaction (3) is unlikely in acidic media although it is proposed for Pt(100) in

alkaline media [5,18,19]. Reaction (3) follows a Langmuir-Hinshelwood recombination

reaction between $NO_{(ad)}$ and $NH_{2(ad)}$ *via* a transient species of N-nitrosamide ($NONH_2$)

[5,7,18,19] and is sensitive to solution pH: the electrocatalytic activity of Pt(100) drops

as the pH decreases and approaches the $pK_a$ of $NH_4^+$ ($pK_a = 9.3$ for $NH_4^+$) [19]. DFT

calculations also suggest that metals with stronger adsorption of $H_{(ad)}$ have lower

activation energy for hydrogenation reactions involving $N_{(ad)}$, $NH_{(ad)}$ and $NH_{2(ad)}$ [45].

This means that metal surfaces with weaker $H_{(ad)}$ adsorption tend to show higher

activation energy for the hydrogenation reactions. Since Pd–Pt(100) has weaker

hydrogen adsorption than Pt(100) (**Fig. 1a**), the formation of $NH_{2(ad)}$ in Reaction (3) can

be expected to be more suppressed at Sn/Pd–Pt(100) than at Pt(100), which allowed us to exclude Reaction (3) as the main reaction pathway for Sn/Pd–Pt(100). Regarding Reaction (4), this mechanism has not been confirmed experimentally yet [7,43] and the contribution of it remains unclear although this reaction is considered as an elementary step to $N_2$ in DFT calculations [15,45].

## 4. Conclusions

Pt(100), Pd(100) and Pd–Pt(100) with 3 at % of Pd electrodes were prepared. Although these electrodes showed almost no activity for the $NO_3RR$ in acidic media, the surface modification with tin activated them for the $NO_3RR$. The quantification of volatile products allowed us to confirm that Sn/Pd(100) and Sn/Pd–Pt(100) produced $N_2$ but Sn/Pt(100) did not. These results indicate that Sn and Pd serve as the promotor for the initial rate-determining step of the $NO_3RR$, $NO_3^-$ to $NO_2^-$, and the selector to $N_2$, respectively. Since Pd–Pt(100) exhibited a weaker affinity with hydrogen adatoms than Pt(100), tuning of hydrogen adsorption energy for metal alloys would be a key to the selective production of dinitrogen. NO is produced as a key intermediate species to the $N_2$ formation and it is highly likely that the NO binding to the electrode surface can be affected by the tin modification: surface availability and NO binding ability. To understand the main reaction pathway for the $NO_3RR$ to $N_2$ at Sn/Pd(100) or Sn/Pd–

22

Pt(100), further electrochemical and spectroscopic studies on not only the NO$_3$RR but also the NO reduction reaction using spectroscopic techniques such as *in situ* FTIR spectroscopy [36,37,46] are needed.

# References

[1] A.R. Ravishankara, J.S. Daniel, R.W. Portmann, Science, **326**, 123-125 (2009).

https://doi.org/10.1126/science.1176985

[2] H. Tian, R. Xu, J.G. Canadell, R.L. Thompson, W. Winiwarter, P. Suntharalingam, E.A. Davidson, P. Ciais, R.B. Jackson, G. Janssens-Maenhout, M.J. Prather, P. Regnier, N. Pan, S. Pan, G.P. Peters, H. Shi, F.N. Tubiello, S. Zaehle, F. Zhou, A. Arneth, G. Battaglia, S. Berthet, L. Bopp, A.F. Bouwman, E.T. Buitenhuis, J. Chang, M.P. Chipperfield, S.R.S. Dangal, E. Dlugokencky, J.W. Elkins, B.D. Eyre, B. Fu, B. Hall, A. Ito, F. Joos, P.B. Krummel, A. Landolfi, G.G. Laruelle, R. Lauerwald, W. Li, S. Lienert, T. Maavara, M. MacLeod, D.B. Millet, S. Olin, P.K. Patra, R.G. Prinn, P.A. Raymond, D.J. Ruiz, G.R. van der Werf, N. Vuichard, J. Wang, R.F. Weiss, K.C. Wells, C. Wilson, J. Yang, Y. Yao, Nature, **586**, 248-256 (2020).

https://doi.org/10.1038/s41586-020-2780-0

[3] W.C. Trogler, Coord. Chem. Rev., **187**, 303-327 (1999).

https://doi.org/10.1016/S0010-8545(98)00254-9

[4] K.A. Karanasios, I.A. Vasiliadou, S. Pavlou, D.V. Vayenas, J. Hazard. Mater., **180**, 20-37 (2010).

https://doi.org/10.1016/j.jhazmat.2010.04.090

[5] M. Duca, M.T.M. Koper, Energy Environ. Sci., **5**, 9726-9742 (2012).

https://doi.org/10.1039/C2EE23062C

[6] Y. Zeng, C. Priest, G. Wang, G. Wu, Small Methods, **4**, 2000672 (2020).

https://doi.org/10.1002/smtd.202000672

[7] S. Garcia-Segura, M. Lanzarini-Lopes, K. Hristovski, P. Westerhoff, Appl. Catal. B: Environ., **236**, 546-568 (2018).

https://doi.org/10.1016/j.apcatb.2018.05.041

[8] N. Singh, B.R. Goldsmith, ACS Catal., **10**, 3365-3371 (2020).

https://doi.org/10.1021/acscatal.9b04167

[9] J. Yang, M. Duca, K.J.P. Schouten, M.T.M. Koper, J. Electroanal. Chem., **662**, 87-92 (2011).

https://doi.org/10.1016/j.jelechem.2011.03.015

[10] M. Kato, M. Okui, S. Taguchi, I. Yagi, J. Electroanal. Chem., **800**, 46-53 (2017).

https://doi.org/10.1016/j.jelechem.2017.01.020

[11] J. Yang, F. Calle-Vallejo, M. Duca, M.T.M. Koper, ChemCatChem, **5**, 1773-1783 (2013).

https://doi.org/10.1002/cctc.201300075

[12] S. Piao, Y. Kayama, Y. Nakano, K. Nakata, Y. Yoshinaga, K. Shimazu, J. Electroanal. Chem., **629**, 110-116 (2009).

https://doi.org/10.1016/j.jelechem.2009.01.031

[13] Y.Y. Birdja, J. Yang, M.T.M. Koper, Electrochim. Acta, **140**, 518-524 (2014).

https://doi.org/10.1016/j.electacta.2014.06.011

[14] K. Shimazu, R. Goto, S. Piao, R. Kayama, K. Nakata, Y. Yoshinaga, J. Electroanal. Chem., **601**, 161-168 (2007).

https://doi.org/10.1016/j.jelechem.2006.11.005

[15] H.-J. Chun, V. Apaja, A. Clayborne, K. Honkala, J. Greeley, ACS Catal., **7**, 3869-3882 (2017). https://doi.org/10.1021/acscatal.7b00547

[16] D. Skachkov, C. Venkateswara Rao, Y. Ishikawa, J. Phys. Chem. C, **117**, 25451-25466 (2013). https://doi.org/10.1021/jp4048874

[17] H. Li, Y. Li, M.T.M. Koper, F. Calle-Vallejo, J. Am. Chem. Soc., **136**, 15694-15701 (2014). https://doi.org/10.1021/ja508649p

[18] M. Duca, M.C. Figueiredo, V. Climent, P. Rodriguez, J.M. Feliu, M.T.M. Koper, J. Am. Chem. Soc., **133**, 10928-10939 (2011).
https://doi.org/10.1021/ja203234v

[19] M. Duca, M.O. Cucarella, P. Rodriguez, M.T.M. Koper, J. Am. Chem. Soc., **132**, 18042-18044 (2010).
https://doi.org/10.1021/ja1092503

[20] A.C.A. de Vooys, M.T.M. Koper, R.A. van Santen, J.A.R. van Veen, J. Catal., **202**, 387-394 (2001). https://doi.org/10.1006/jcat.2001.3275

[21] B. Wang, X.-y. Li, Anal. Chem., **70**, 2181-2187 (1998). https://doi.org/10.1021/ac970601h

[22] A. Kudo, A. Mine, J. Electroanal. Chem., **408**, 267-269 (1996). https://doi.org/10.1016/0022-0728(96)04630-X

[23] K.H. Kim, T. Lim, M.J. Kim, S. Choe, S. Baek, J.J. Kim, Electrochem. Commun., **62**, 13-16 (2016). https://doi.org/10.1016/j.elecom.2015.11.002

[24] N. Todoroki, H. Tsurumaki, H. Tei, T. Mochizuki, T. Wadayama, J. Electrochem. Soc., **167**, 106503 (2020).
https://doi.org/10.1149/1945-7111/ab9960

[25] Y. Qu, L. Wang, C. Li, Y. Gao, J. Kyong Sik, J. Rao, G. Yin, Int. J. Hydrog. Energy, **42**, 228-235 (2017).
https://doi.org/10.1016/j.ijhydene.2016.08.215

[26] A. Zolfaghari, G. Jerkiewicz, J. Electroanal. Chem., **420**, 11-15 (1997). https://doi.org/10.1016/S0022-0728(96)01020-0

[27] J. Clavilier, J.M. Feliu, A. Fernandez-Vega, A. Aldaz, J. Electroanal. Chem. Interf. Electrochem., **269**, 175-189 (1989).
https://doi.org/10.1016/0022-0728(89)80111-1

[28] D.J. Watson, G.A. Attard, Surf. Sci., **515**, 87-93 (2002). https://doi.org/10.1016/S0039-6028(02)01811-3

[29] S. Motoo, N. Furuya, Berichte der Bunsengesellschaft für physikalische Chemie, **91**, 457-461 (1987).
https://doi.org/10.1002/bbpc.19870910446

[30] N. Hoshi, K. Kagaya, Y. Hori, J. Electroanal. Chem., **485**, 55-60 (2000). https://doi.org/10.1016/S0022-0728(00)00098-X

[31] N. Hoshi, M. Kuroda, O. Koga, Y. Hori, J. Phys. Chem. B, **106**, 9107-9113 (2002).

https://doi.org/10.1021/jp020898+

[32] K. Sashikata, Y. Matsui, K. Itaya, M.P. Soriaga, J. Phys. Chem., **100**, 20027-20034 (1996).

https://doi.org/10.1021/jp9620532

[33] M. Wakisaka, Y. Hyuga, K. Abe, H. Uchida, M. Watanabe, Electrochem. Commun., **13**, 317-320 (2011).

https://doi.org/10.1016/j.elecom.2011.01.013

[34] F.J. Vidal-Iglesias, A. Al-Akl, D. Watson, G.A. Attard, J. Electroanal. Chem., **611**, 117-125 (2007).

https://doi.org/10.1016/j.jelechem.2007.08.005

[35] K. Tada, K. Shimazu, J. Electroanal. Chem., **577**, 303-309 (2005).

https://doi.org/10.1016/j.jelechem.2004.11.039

[36] B. Álvarez, A. Rodes, J.M. Pérez, J.M. Feliu, J.L. Rodríguez, E. Pastor, Langmuir, **16**, 4695-4705 (2000).

https://doi.org/10.1021/la991473q

[37] I. Katsounaros, M.C. Figueiredo, X. Chen, F. Calle-Vallejo, M.T.M. Koper, ACS Catal., **7**, 4660-4667 (2017).

https://doi.org/10.1021/acscatal.7b01069

[38] I. Katsounaros, M.C. Figueiredo, X. Chen, F. Calle-Vallejo, M.T.M. Koper, Electrochim. Acta, **271**, 77-83 (2018).

https://doi.org/https://doi.org/10.1016/j.electacta.2018.03.126

[39] J. Yang, Y. Kwon, M. Duca, M.T.M. Koper, Anal. Chem., **85**, 7645-7649 (2013).

https://doi.org/10.1021/ac401571w

[40] K. Nishimura, K. Machida, M. Enyo, Electrochim. Acta, **36**, 877-880 (1991).

https://doi.org/10.1016/0013-4686(91)85288-I

[41] G.E. Dima, A.C.A. de Vooys, M.T.M. Koper, J. Electroanal. Chem., **554-555**, 15-23 (2003).

https://doi.org/10.1016/S0022-0728(02)01443-2

[42] A. Clayborne, H.-J. Chun, R.B. Rankin, J. Greeley, Angew. Chem. Int. Ed., **54**, 8255-8258 (2015).

https://doi.org/10.1002/anie.201502104

[43] I. Katsounaros, G. Kyriacou, Electrochim. Acta, **53**, 5477-5484 (2008).

https://doi.org/10.1016/j.electacta.2008.03.018

[44] M.T. de Groot, M.T.M. Koper, J. Electroanal. Chem., **562**, 81-94 (2004).

https://doi.org/10.1016/j.jelechem.2003.08.011

[45] J.-X. Liu, D. Richards, N. Singh, B.R. Goldsmith, ACS Catal., **9**, 7052-7064 (2019).

https://doi.org/10.1021/acscatal.9b02179

[46] J. Souza-Garcia, E.A. Ticianelli, V. Climent, J.M. Feliu, Electrochim. Acta, **54**, 2094-2101 (2009).

https://doi.org/10.1016/j.electacta.2008.08.059

**Graphical abstract**
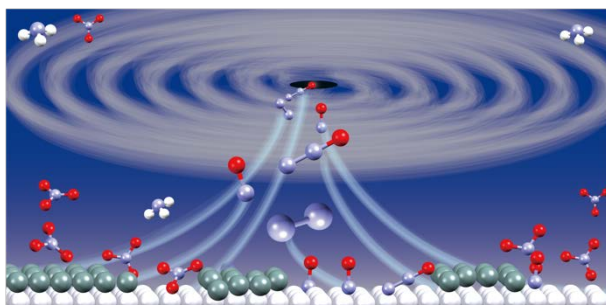


**Highlights**

- Sn/Pt(100), Sn/Pd(100) and Sn/Pd–Pt(100) were prepared for the nitrate reduction.

- Gasous products for the electrochemical $NO_3RR$ were analyzed using OLEMS.

- Sn/Pd(100) and Sn/Pd-Pt(100) produced $N_2$ but not Sn/Pt(100).